Journal of Applied Fluid Mechanics, Vol. 17, No. 5, pp. 1002-1014, 2024.
Available online at www.jafmonline.net, ISSN 1735-3572, EISSN 1735-3645.
https://doi.org/10.47176/jafm.17.05.2287

Numerical Simulation of Inverted Bucket Steam Valve Noise based on Multiband Analysis

M. Zhao, D. Liu†, J. Hou, X. Zhang and S. Li

Lanzhou University of Technology, Lanzhou, 730050, China
Machinery Industry Pump Special Valve Engineering Research Center, Lanzhou, 730050, China

†Corresponding Author Email: 222085802017@lut.edu.cn

ABSTRACT

As an important control element in steam heating piping systems, the safety and stability of inverted bucket steam valves determine the reliable operation of the system. Therefore, it is necessary to investigate the acoustic mechanism of inverted bucket steam valves. Aiming at the difficulty of numerical simulation in accurately predicting the aerodynamic noise of inverted bucket steam valves, this paper proposes a new method for simulating the aerodynamic noise of inverted bucket steam valves based on multiband analysis (LES). The flow field of the inverted bucket steam valve is numerically simulated using the LES method to obtain wall pressure pulsation information and fluid velocity pulsation information, which are used as excitation sources for acoustic simulation. The characteristics of dipole and quadrupole sound sources were obtained by applying the FW-H method and experimentally verified. The results show that a new multifrequency band analysis method for inverted bucket steam valves is effective by comparing the numerical simulation results, in which the dipole source dominates in the low-frequency band, in the medium frequency range, the quadrupole source outperforms the dipole source, but in the high frequency range, the quadrupole source is dominant. The experimental results are in good agreement with the simulation results, and the correctness of the numerical simulation is confirmed by the fact that there is less than a 3% difference between the findings of the numerical simulation and the experimental data.

Article History

Received September 6, 2023
Revised December 12, 2023
Accepted December 16, 2023
Available online February 24, 2024

Keywords:

Valve
Acoustical
Frequency division
Dipole and quadrupole
Sound source characteristics

1. INTRODUCTION

Steam, as one of the world's major energy supply resources has a wide range of applications in industrial production. However, with the promotion of the national "dual-carbon" goal and the green and high-quality development policy, the importance and urgency of energy conservation and efficiency improvement in the industrial field are becoming increasingly prominent. Therefore, optimizing the level of energy consumption of steam systems is now a pressing issue that needs to be resolved (Li et al., 2012; Qiu et al., 2023). Practice has shown that the effectiveness of valve use has a critical impact on steam system energy savings, sometimes accounting for as much as 50% of the energy-saving potential of a steam system. As one of the main structural forms of steam valves, inverted bucket steam valves, when the fluid passes through the valve internals at the throttling point, the pressure decreases drastically, which not only causes energy loss in the entire piping system, but also impacts the valve body, causes vibration and noise, and shortens the service life of the valve (Huang et al., 2014). Therefore, the study of flow-induced noise in steam valves is of great academic value and engineering significance.

Few studies have been done to date on the use of LES and CFD techniques to predict the aerodynamic noise of inverted bucket steam valves, and the accuracy of numerical simulation of aerodynamic noise cannot be guaranteed. Liu et al. (2018) simulated the aerodynamic noise of butterfly valves numerically using a combination of CFD and acoustic tools, and the findings demonstrated that the butterfly valve aerodynamic noise's sound pressure level spectrum was broad and lacked a clear primary frequency. Liao et al. (2022) investigated a combination of CFD and CAA methods to simulate the aerodynamic noise of eccentric rotary valves, and the outcomes demonstrated that there was only a 3 dB (A) difference between the experimental and simulated sound

NOMENCLATURE

σ_{ij}	stress tensor	$H(f)$	Heaviside function
τ_{ij}	sublattice scale stress tensor	N	number of frequency samples
v_i	moving velocity component of the integration surface	n_i	sound pressure at the sampling frequency point
δ_{ij}	Kronecker function	p	filtering pressure
$\delta(f)$	Dirac function	p_0	the pressure exerted on the fluid when undisturbed
ρ	fluid density	P'	sound pressure at the observation point
ρ_0	fluid density when undisturbed	T_{ij}	Lighthill stress tensor
a_0	far-field sound velocity	t	time
c_0	speed of sound	u_i	fluid velocity component in the direction
e_{ij}	viscous stress tensor	x	spatial coordinates

pressure levels. Shi et al. (2023) investigated the aerodynamic noise of a marine three-way control valve based on fluid-solid coupling theory. However, none of them considered the effect of different frequency bands on the numerical simulation of noise when they performed a numerical simulation of aerodynamic noise, meaning that the current study is meaningful.

The theory of valve acoustics and numerical simulation have been extensively studied in recent years by academics both domestically and internationally. Dai et al. (2022) studied a small high-speed centrifugal fan as the research object and examined the process by which aerodynamic noise is generated. The results showed that the sound sources of valves, high-speed centrifugal fans, and other equipment are mainly composed of dipole and quadrupole sound sources. Mori et al. (2017) carried out simulation and experimental research on aerodynamic noise in T-shaped, rectangular pipes with walls that are between 2 and 5 mm thick. The findings demonstrated that the fluid flow rate in the pipeline has a major impact on the aerodynamic noise sound source characteristics, and the pipeline's vibration and acoustic properties mostly influence the sound field features. Yuan et al. (2017) studied on the influence of the nozzle structure and arrangement parameters of the closed vessel of the equipment on the three nozzles on the steam underwater injection noise, and a steam underwater injection noise model was established based on the theoretical analysis and test results. The results showed that at atmospheric pressure, the steam underwater injection noise gradually increases with increasing water temperature and then decreases rapidly. The zone with water temperatures between 55 ℃ and 75 ℃ has the most injection noise, and the nozzle construction has the least impact on it. Wu et al. (2023) simulated the noise at one meter outside the pipe wall behind the steam engine bypass valve numerically and calculated the noise theoretically. The findings demonstrated that there is only a 0.94dB(A) discrepancy between the theoretical calculation data and the numerical simulation data, confirming the correctness of the noise simulation method. Wang et al. (2007) used numerical simulation to examine the steam flow and noise radiation in a steam turbine's main steam regulating valve. The findings indicated that the dead zone in the valve cavity and the strong eddy volume region near the valve throat were the primary locations of noise (Si et al., 2018). The internal acoustic field of a centrifugal pump is solved using computational fluid dynamics (CFD) and computational acoustics (CA), which is based on the Lighthill acoustic simulation theory. The results showed that the numerical simulation data obtained by the acoustic boundary element method have a maximum error value of less than 5.3 dB compared with the experimental data, and it can take into account a variety of turbulent noise sources with high simulation accuracy. Xu et al. (2010) employed a numerical simulation technique that combined CFD and CAA to analyze the main steam isolation valve's vibration and noise caused by turbulence quantitatively. The results showed that the large eddy simulation algorithm can reveal the spectral characteristics of turbulence which is valuable for turbulence excitation. Based on the fluid-solid one-way fluid structure interaction, (Li et al., 2018) numerical models of a high-pressure bucket valve's flow-excited vibration characteristics and valve piping using CFD software and LMS software. The results showed that the flow-induced vibration spectral characteristics of the valve are determined by the structure of the throttling element inside the valve and are less affected by the change in valve opening. Li & Guo (2012) studied on the mechanism of aerodynamic noise of high-pressure steam valves as well as the prediction method. The results showed that the large-eddy simulation method is suitable for the prediction of aerodynamic noise. Hou et al. (2023) performed noise experiments and examined the balancing valve's sound source characteristics in various frequency ranges. The findings demonstrated that there is a 5% or less difference between the test and simulation data, and the curve trend is essentially the same, confirming the numerical simulation's correctness. Liu et al. (2013) examined the high-speed train's aerodynamic noise source characteristics in a vacuum tube and conducted experimental verification. The results demonstrated that there is a 2.62 dB(A) difference between the experimental and numerical simulation data, indicating that the Lighthill acoustic simulation theory is appropriate for the numerical simulation of aerodynamic noise and that the LES is appropriate for the numerical simulation of the flow field. Xu & He (2017) evaluated the aerodynamic noise generated by the aircraft loop control piping system's butterfly valve plate using the CFD hybrid acoustic finite element approach and the K-FWH integral method. The K-FWH integral method ignores the impact of piping and valve structure on aerodynamic noise, so the CFD hybrid acoustic finite element method is more appropriate for numerical simulation of aerodynamic noise, according to the results, which also showed that the

difference in sound pressure level between the two methods is less than 5%. Tao et al., (2020) examined the pipe flow noise's sound source properties using the FW-H acoustic analogy theory. The results showed that at high fluid flow rates, the sound power of dipole sources is negligible compared to quadrupole sources. Mori et al. (2014) simulated the flow acoustic pressure using the Lighthill acoustic analogy of the boundary element method and verified it in comparison with the experimental data. The outcomes demonstrated that there is a strong correlation between the simulated and experimental data.

In summary, there are fewer studies on the numerical simulation of aerodynamic noise in inverted bucket steam valves. Considering the harmfulness of noise generated by steam valves, to analyze the noise of inverted bucket steam valves based on different frequency bands, a technique for numerical simulation is offered. To verify the numerical simulation method's correctness, the properties of the sound source in various frequency bands and the distribution of sound pressure levels under various operating situations are analyzed.

2. THEORETICAL

2.1 Flow Field Simulation Theory

The acoustic field and the flow are combined in the flow acoustics problem. The N-S equation is the fundamental set of governing equations that describe the flow field inside a steam valve in a nonstationary state, as shown in Eqs. (1-3):

$$\frac{\partial \rho}{\partial t}+\frac{\partial(\rho u_i)}{\partial x_i}=0 \tag{1}$$

$$\frac{\partial(\rho u_i)}{\partial t}+\frac{\partial（\rho u_i u_j）}{\partial x_i}=-\frac{\partial p}{\partial x_i}+\frac{\partial e_{ij}}{\partial x_j} \tag{2}$$

$$e_{ij}=\mu\left(\frac{\partial u_i}{\partial x_j}+\frac{\partial u_j}{\partial x_i}-\frac{2}{3}\delta_{ij}\frac{\partial u_k}{\partial x_k}\right) \tag{3}$$

e_{ij} is the viscous stress tensor, N/m^2; δ_{ij} is the Kronecker function, δ_{ij} =1 for i=j; and δ_{ij} =0 for $i\neq j$. The near-field region is both the sound source and sound propagation region and a set of nonlinear equations can be used to characterize the flow process. The far-field region can be regarded as an acoustic propagation region, and the acoustic field can be described by the Helmholtz equation. There are two categories of numerical computation techniques for steam valve flow noise: direct method and indirect method. To find the physical solution of the flow and acoustic fields, the direct technique solves the system of equations, but it requires a high-precision turbulence model and a large amount of computation, so it is still difficult to realize the direct solution for the flow-induced noise of steam valves. The theoretical basis of the indirect method is derived from the equation (Wu et al., 2022).

The theory of flow-induced noise is a development of the basic equations of acoustics, and the basic equations of flow-induced noise (Lighthill's equations) are derived without any assumptions and simplifications by Lighthill on the equations. He took the hydrodynamic term as the sound source term on one side, which is exactly in the same form as the form of fluctuation equations of classical acoustics. The Reynolds average Navier-Stokes (RANS) approach is unsuitable for noise prediction since it only yields time-averaged data on turbulent pulsations. The LES approach is employed for the numerical computation of the transient flow field since the Direct Numerical Simulation (DNS) solution criteria are more difficult to meet with the available computer resources. The LES technique treats the huge eddies in the energy-containing part of the turbulence differently from the tiny eddies in its dissipative section. While a sublattice model is used to link the small-scale eddies to the large-scale eddies, the large-scale eddy structure is solved directly using the equations. Filtering the nonconstant equations yields the control equations for the large eddy simulation. This procedure efficiently removes minor eddies whose sizes are smaller than the filter width (Sim et al., 2020). The filtered large eddy simulation equation is shown in Eqs. (4-5):

$$\frac{\partial \rho}{\partial t}+\frac{\partial \rho}{\partial x_i}(\rho\bar{u}_i)=0 \tag{4}$$

$$\frac{\partial}{\partial t}(\rho\bar{u}_i)+\frac{\partial}{\partial x_j}(\rho\bar{u}_i\bar{u}_j)=\frac{\partial}{\partial x_j}(u\frac{\partial\sigma_{ij}}{\partial x_j})-\frac{\partial\bar{p}}{\partial x_i}-\frac{\partial\tau_{ij}}{\partial x_j} \tag{5}$$

in Eq: u_i is the value of the x_i direction filtering speed, $\bar{p}$ is the filtering pressure, τ_{ij} is the sublattice scale stress tensor, N/m^2; σ_{ij} is the stress tensor, N/m^2.

2.2 Acoustical Analogy Theory

The acoustic analogy theory was put forth by Lighthill in his investigation of jet free turbulence sound. Guo et al., (2021) relies on the principle of acoustic analogies to replicate the radiation properties of the steam valve's sound source, whose equations can be represented by Eq. (6-7):

$$T_{ij}=\pi_{ij}-\overset{o}{\pi}_{ij}=\rho u_i u_j+\left[(p-p_0)-c_0^{\,2}(\rho-\rho_0)\right]\delta_{ij}-\tau_{ij} \tag{6}$$

$$\frac{\partial^2 p'}{c_0^2\partial t^2}-\nabla^2 p'=\frac{\partial}{\partial t}\left\{\left[\rho_0 v_n+\rho(u_n-v_n)\right]+\delta(f)\right\}-\frac{\partial}{\partial t}\left\{\left[\tau_{ij}n_j+\rho u_i(u_n-v_n)\right]+\delta(f)\right\}+\frac{\partial^2}{\partial x_i\partial x_j}\left[T_{ij}H(f)\right] \tag{7}$$

T_{ij} is the Lighthill stress tensor, N/m^2; ρ is the fluid density, kg/m^3; ρ_0 is the fluid density when undisturbed, kg/m^3; u is the velocity; p is the pressure exerted on the fluid; p_0 is the pressure exerted on the fluid when undisturbed; and c_0 is the speed of sound. t is the time, x is the spatial coordinate, and the indices i and j denote the direction components of the coordinate axes. The Heaviside function is $H(f)$, while the Dirac function is $\delta(f)$. The quadrupole sound source produced by flow turbulence is represented by the third term in Eq. (7), On the right side, the first component represents the monopole sound source created by surface acceleration or displacement

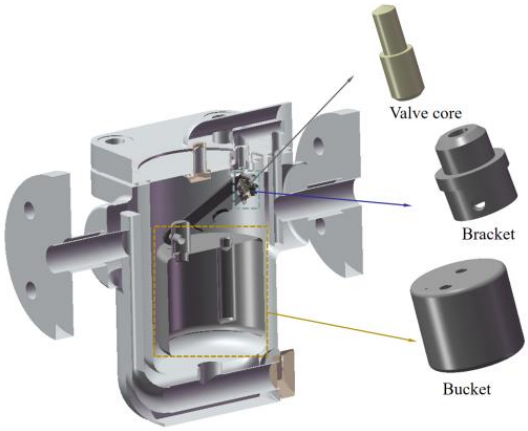

Fig. 1 Schematic structure of inverted bucket steam valve

distribution, while the second term represents the dipole sound source caused by surface pressure perturbation. A monopole source implies a radiated sound source associated with a vacuole, while a dipole source and a quadrupole source are used to describe a nonvacuum radiated sound source. The steam valve medium is water vapor, which basically does not undergo cavitation, so the steam valve sound source is a combination of a dipole source and a quadrupole source.

Farassat created the FW-H acoustic fluctuation equation from the Lighthill equation, Ffowcs Williams, Hawkings and others to obtain the FW-H acoustic fluctuation equation, as is now seen in Eq.(8):

$$\frac{1}{a_0}\frac{\partial p'}{\partial t^2}-\nabla^2 p'=\frac{\partial}{\partial t}\left\{\left[p_0 v_n+p(u_n-v_n)\right]\delta(f)\right\}- \\ \frac{\partial}{\partial x_i}\left\{\left[p_{ij}n_j+pu_i(u_n-v_n)\right]\delta(f)\right\}+\frac{\partial^2}{\partial x_i \partial x_j}(T_{ij}H(f)) \tag{8}$$

where *ui* denotes the component of fluid velocity in the direction; the moving velocity component of the integration surface is denoted by a_0, and the fluid velocity components perpendicular to it is v_i; P' is the sound pressure at the observation point; and the Heaviside function is $H(f)$, while the Dirac function is $\delta(f)$. The source's surface distribution is represented by $\delta(f)$ for thickness and loading source terms, while its volume distribution is represented by $H(f)$ for the quadrupole source. The inclusion of $H(f)$ and $\delta(f)$ in the equations ensures that the FW-H equations hold throughout the unbounded space; τ_{ij} and T_{ij} are the stress tensor and the Lighthill tensor, respectively.

3. Establishment of an Inverted Bucket Steam Valve Model and Simulation of a Flow Field

A PN40 DN25 inverted bucket steam valve was used as the object of study. PN40 means that the analysed inverted bucket steam valve can withstand a pressure 40 times that of standard atmospheric pressure, and DN25 means the average inner diameter of the valve. The basic principle of operation is to use the density difference between the condensate and steam to make the inverted bucket generate upward buoyancy to achieve valve closure. Its structure is shown in Fig. 1, it is made up of the valve body, cover, bucket, seat, valve core, and other parts in its whole.

Table 1 Inverted bucket steam valve parameters

Name	Inverted Bucket Steam valves
Fluid media	Water vapor/condensate
Nominal pressure	PN40
Nominal Diameter	DN25
Maximum working pressure	2.5MPa
Valve Materials	A216 WCB

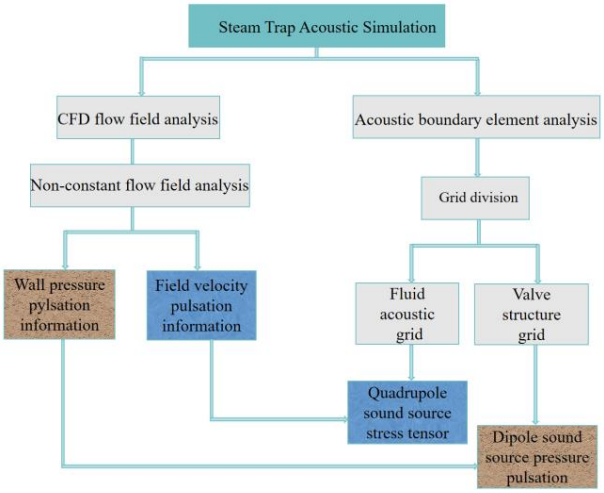

Fig. 2 Simulation process

The main technical parameters of the inverted bucket steam valves are shown in Table 1. A216 WCB is cast carbon steel, selected for valve bodies, barrels, brackets, and FXM-19 is austenitic stainless steel, selected for valve core.

3.1 Simulation and Modeling Calculation Process

In Fig. 2, the simulation procedure is displayed.

3.2 Flow Field Simulation Calculation

To realize high-precision CFD flow field simulation, the 3D geometric model of the inverted bucket steam valve is reasonably simplified under the premise of guaranteeing the calculation accuracy and retaining the detailed features of the model (Tan et al., 2023). To ensure that the fluid inlet flow is stable and the turbulent flow at the outlet is fully developed, the piping at the inlet end of the valve is extended to five times the nominal diameter, and the piping at the outlet end of the valve is extended to ten times the nominal diameter (Yan et al., 2023). To make sure that the fluid flows through the valve sufficiently to gather more precise data about the flow field, the piping is extended at the valve's inlet and outlet ends (Wang et al., 2013). Secondly, the accuracy of the flow field computation is impacted by a suitable mesh division. Figure 3 depicts the mesh partition of an inverted bucket

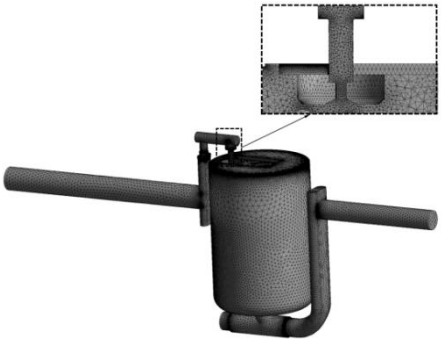

Fig. 3 Inverted bucket steam valve runner mesh model

steam valve's flow channel. In the meshing process, the shape of the runner in the inverted bucket steam valve model is complex, so a hybrid tetrahedral/hexahedral mesh is used to mesh the runner model (Gao et al., 2023). The comprehensive number of grids and the requirements of the solution accuracy when the flow is relatively smooth and contains less information about the flow field can ensure the calculation accuracy and it is capable of appropriately reducing the number of grids to shorten the computation's duration. After grid-independence validation, the total number of grids used is 3061921. For calculating the flow field of an inverted bucket steam valve, the fluid medium is set to be water, with a temperature of 80 degrees Celsius, with a viscosity coefficient of 0.000357kg/(m·s) and a density of 971.8kg/m^3.

Figures 4-6 show the transient flow field's pressure cloud flow line diagrams at a pressure drop of 0.8MPa.

As shown in Fig .4-Fig. 5, the steam valve before and after the valve flow rate is uniform, the valve seat core is due to the jet flow pressure attenuation, the highest flow rate is 53.5 m/s^2, and the steam sprayed with the wall after the momentum change is caused by the flow of solid-coupled surface pressure pulsation of the dipole sound source. From Fig. 6, the combination of the throttling movement, the valve seat, and the jet effect generated by the back area results in a quadrupole sound source. Thus, the noise source of the inverted bucket steam valve that is the focus of this study is created by the combination of the dipole and quadrupoe sound sources.

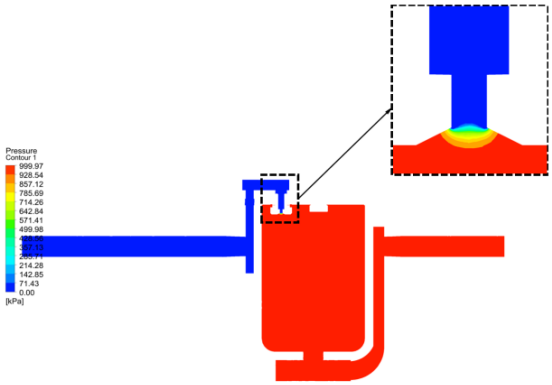

Fig. 4 Pressure cloud of flow field simulation

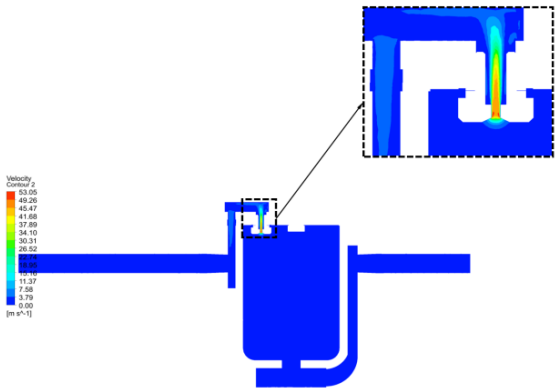

Fig. 5 Velocity cloud for flow field simulation

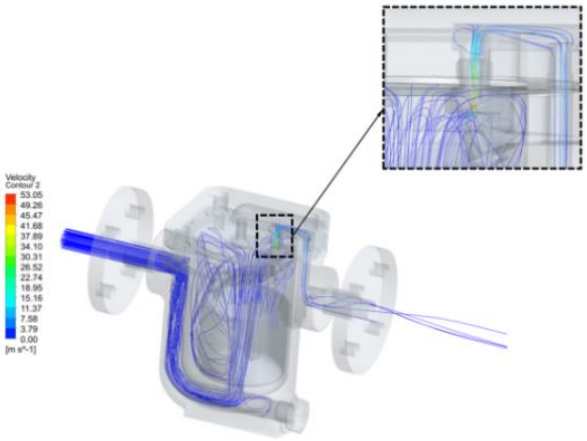

Fig. 6 Streamline diagram of the flow field simulation

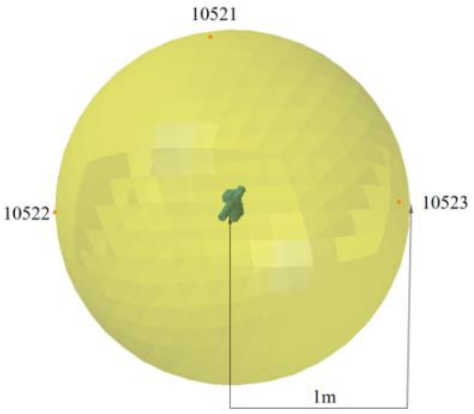

Fig. 7 Schematic diagram of the course monitoring points

4. Acoustic Simulation

4.1 Boundary Conditions for Acoustic Simulation

The acoustic coupling is computed using software that combines CFD and LMS Virtual Lab together. The wall pressure pulsation information obtained from the flow field calculation is mapped onto the grid of acoustic boundary elements as an energy loss-free layout. As seen in Fig. 7, the far-field monitoring point was established, and the dipole sound source's time-domain data was subjected to the Fourier transform. Get the dipole pressure

(a) 2520 Hz pressure pulsation map

(b) 4520 Hz pressure pulsation map

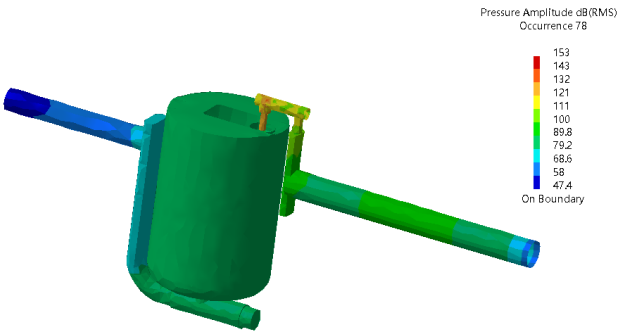

(c) 6120 Hz pressure pulsation map

(d) 7120 Hz pressure pulsation map

Fig. 8 Inverted bucket steam valve pressure pulsation graphs at different frequencies

pulsation cloud maps at different frequencies, as shown in Fig. 8, the time-domain data from the quadrupole sound source were subjected to the Lighthill stress tensor analysis. Figure 9 displays quadrupole stress tensor distribution cloud maps at various frequencies**,** with the acquisition frequency set from 20 to 8000 Hz and the step size set to 50 Hz.

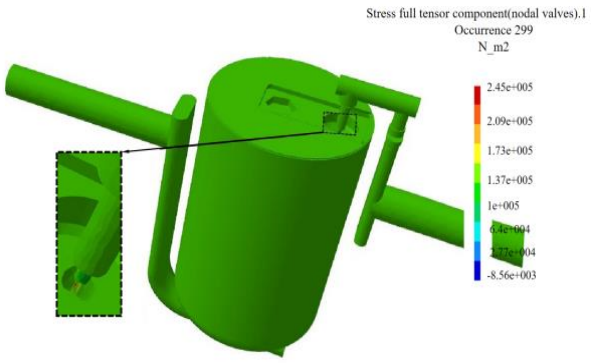

(a) 3000Hz quadrupole stress tensor distribution map

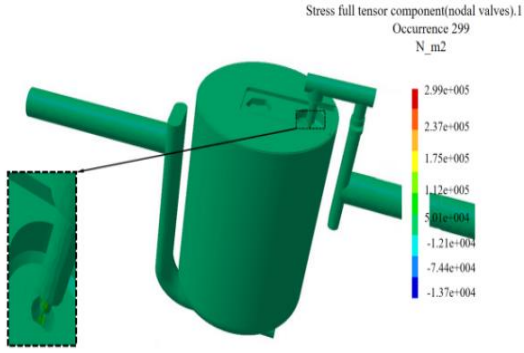

(b) 5200Hz quadrupole stress tensor distribution map

Fig. 9 Inverted bucket steam valve quadrupole stress tensor distribution graphs at different frequencies

4.2 Acoustic Simulation

The fluid's contact with the solid wall causes a change in the fluid's pressure at the wall, which creates the dipole, so the pressure pulsation at the solid surface can be used to describe the dipole sound source intensity. For this purpose, by processing the mesh mapping, the pressure pulsation information of the flow field is transferred to the inner wall surface of the shell without requiring any energy loss to obtain the dipole sound source distribution information. The spherical sound field cloud of the steam valve at typical frequencies is taken to obtain the dipole level sound field distribution for different operating conditions, as shown in Fig. 10. From the cloud view of the spherical sound field at 3000Hz, 5500Hz etc., the dipole sound source shows a typical symmetrical distribution, and at a frequency of 3000Hz, while at 74.1 dB (A), it corresponds to a maximum sound pressure value, at a frequency of 5500Hz, the steam valve's spherical sound field to a maximum sound pressure value of 70.3dB(A).

when there is a 0.8MPa pressure differential, the three sound pressure monitoring points are denoted 10521, 10522 and 10523, as shown in Fig. 11, which displays the three monitoring stations' sound pressure level curves. The sound pressure exhibits a rising, stable, and eventually dropping tendency. The peak sound pressure level is 73.47dB(A) at a pressure differential of 0.8Mpa. The noise's dominating frequencies are 1250Hz and 1470Hz.

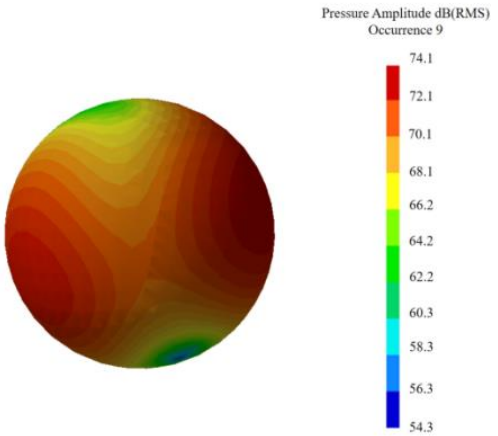

(a)3000Hz dipole sound pressure contour

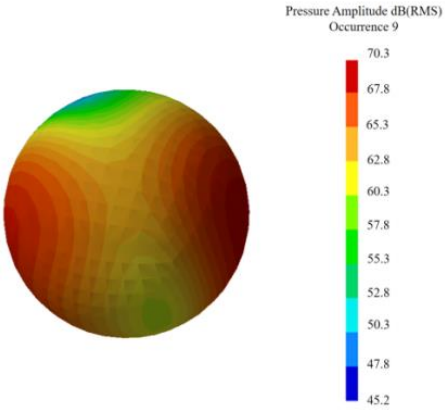

(b) 5500Hz dipole sound pressure contour

Fig. 10 Sound pressure curve of dipole at typical frequencies

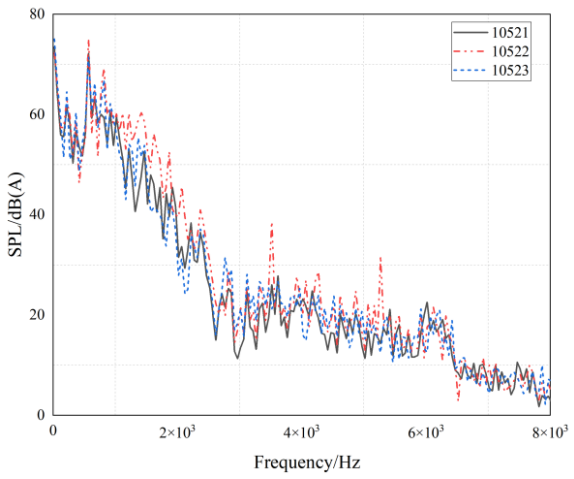

Fig. 11 Dipole sound pressure level curves at various points of observation

Quadrupoles are generated by turbulent motion due to viscous shear stresses in the fluid, so the stress tensor can be used to represent the quadrupole sound source intensity. The turbulence information of the flow channel mesh is transferred to the acoustic mesh in the flow field

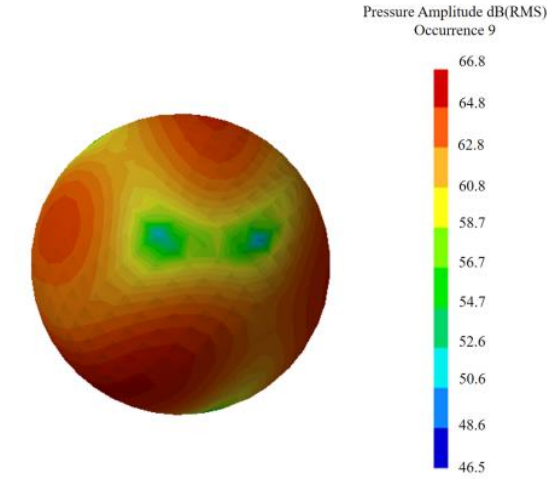

(a) 1020Hz quadrupole sound pressure contour

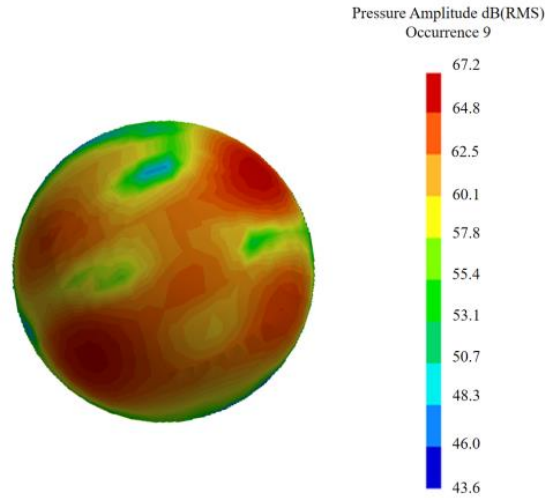

(b) 2000Hz quadrupole sound pressure contour

Fig. 12 Sound pressure curve of quadrupole at typical frequencies

by the mesh mapping process via the Lighthill transform principle. The spherical acoustic field cloud of the steam valve at typical frequencies is obtained as the distribution of the quadrupole acoustic field under different operating conditions. As shown in Fig. 12, from the spherical distribution cloud diagrams of 1020Hz, 2000Hz, etc., the quadrupole has a canonical distribution. The steam valve's spherical sound field has a maximum sound pressure value of 66.8 dB(A) at 1020 Hz and the steam valve's spherical sound field has a maximum sound pressure value of 67.2 dB(A) at 2000 Hz.

As illustrated in Fig. 13, the three sound pressure monitoring locations are designated 100521, 100522, and 100523, when the pressure difference is 0.8Mpa, it displays the three monitoring stations' sound pressure level graphs. First. There is an increasing trend in the sound pressure, steady, and then falling. The highest sound pressure level is 62.09dB(A) at a pressure differential of 0.8Mpa. The major noise frequencies are 770Hz and 1270Hz.

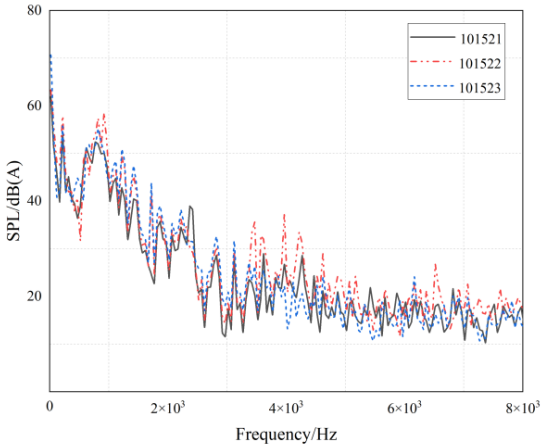

Fig. 13 Quadrupole sound pressure level curve at several points of observation

Table 2 ΔP=0.8MPa Sound pressure levels at monitoring points

working condition	Δ P=0.8MPa			
sound pressure monitoring point	10521	10522	10523	Total Sound Pressure level (TSP)
SPL/dB(A)	61.35	66.51	65.45	64.44

The sound pressure spectrogram at each monitoring location is unique. Nonetheless, the distribution of sound pressure levels often follows a consistent trend. Eq. (8) displays the superposition formula for the sound pressure readings superimposed from several sound pressure monitoring locations:

N is the number of frequency samples, and n_i is the sound pressure at the sampling frequency point.

Table 2 shows that the difference between monitoring points 10521 and monitoring point 10522 is 5.16 dB(A), and the difference between monitoring points 10522 and monitoring point 10523 is 1.06 dB(A). Since the noise generated by reflection and the medium flow state will be considered in the numerical simulation for noise calculation and the acoustic grid will adaptively divide the encryption degree of the grid in the process of dividing, The sound pressure levels at each monitoring location will differ from one another. The arithmetic mean of the sound pressure readings taken at the three sound pressure monitoring stations is used to calculate the overall noise sound pressure level. Or 64.44 dB(A). There is only a 5 dB(A) maximum variance in sound pressure level.

5. MULTIFREQUENCY BAND-BASED ANALYSIS OF DIPOLE AND FOUR-LEVEL SOURCE CHARACTERISTICS

The dipole's noise value is greater than the quadrupole's total noise value when the frequency is between 0 and 2020 Hz, this can be ascertained by

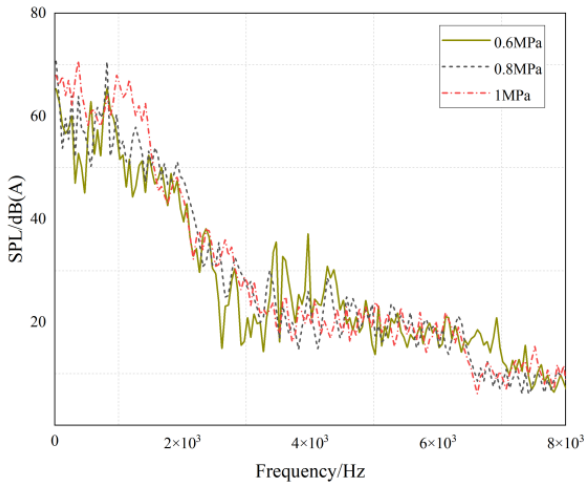

Fig. 14 Comparison of simulated sound pressures at different pressure differentials

contrasting the frequency-dependent dipole sound pressure level in Fig. 11 with the frequency-dependent quadrupole sound pressure level in Fig. 13. When the frequency is within 2020Hz to 6370Hz, the dipole is interleaved with the quadrupole. The noise value of the quadrupole is greater than that of the dipole for frequencies greater than 6370 Hz. Thus, dipole noise from 0~2020Hz dominates the noise of the inverted bucket steam valve; by quadrupole and dipole noise from 2020Hz~6370Hz; and by quadrupole noise at frequencies greater than 6370Hz.

Based on the aforementioned research, a numerical simulation technique based on multifrequency bands is suggested to analyze the noise of inverted bucket steam valves, as shown in Eq. (9), and the numerical simulation

$$L_{pAe}=10\lg\left(10^{\frac{n_1}{10}}+\cdots+10^{\frac{n_i}{10}}+\cdots 10^{\frac{n_N}{10}}\right) \quad (8)$$

comparison diagrams for the three types of differential pressures are shown in Fig. 14.

$$SPL(f)=\begin{cases} SPL_{quard}(f) & 0Hz\le f\le 2020Hz \\ 10\lg\left(10^{\frac{SPL_{quad}(f)}{10}}+10^{\frac{SPL_{dip}(f)}{10}}\right) & 2020Hz\le f\le 6370Hz \\ SPL_{dip}(f) & f\ge 6370Hz \end{cases} \quad (9)$$

Where $SPL_{quad}(f)$ is the sound pressure level for the quadrupole and $SPL_{dip}(f)$ is the sound pressure level for the dipole.

Comparison plot of simulated sound pressure levels for numerical simulations with pressure differences of 0.6MPa, 0.8Mpa, and 1.0MPa.

6. COMPARISON OF EXPERIMENTAL AND SIMULATION RESULTS

6.1 Acoustic Simulation

The inverted bucket steam valve noise platform design is shown in Fig. 15.

Fig. 15 Testing platform

Fig. 16 Acoustic sensor

Fig. 17 Dynamic collector

The KSI-308A213 precision free-field microphone was selected for the noise measurement device, as shown in Fig. 16. The precision free-field microphone has an open-circuit sensitivity (@250Hz) of 50Mv/Pa, frequency range of 20 ~ 20kHz, a dynamic range greater than 146dB, including preamplifiers and other characteristics.

As illustrated in Fig. 17, the vibration and noise test data collecting device chosen is an 8-channel ultrahigh dynamic acquisition instrument from DEWESoft's SIRIUS series. 8-channel ultrahigh SIRIUS series dynamic acquisition instruments with up to 200 kHz per channel of the sampling frequency, the dynamic range of 160 dB @ autoranging, SNR 135 dB @ 50 kHz, support the TEDS intelligent sensors and other features.

6.2 Acoustic Simulation

The noise data of the inverted bucket steam valves was gathered using the noise test software with differential pressures of 0.6MPa, 0.8MPa, and 1.0MPa in 0~2s and to obtain the frequency domain and time domain data under different operating conditions. Due to the influence of the environment at the time of the experiment, there was too much redundant noise, so this paper sets the experimental conditions of the time-frequency analysis before the application of MATLAB software for signal denoising. This function uses the denoising theory for the moving average method, which is a time-domain idea of denoising methods. The primary theory of the algorithm is that the sampling point near the point takes the arithmetic average as the value of this point after the reduction of the noise, to obtain the final reduction of noise after the frequency-domain and time-domain data, as displayed in Fig. 18.

The sound pressure levels for each of the three experimental scenarios were logarithmically superimposed to provide the total sound pressure levels for the three pressure disparities, as Table 3 shows.

6.3 Comparison of Experimental and Simulation Results

A comparison of inverted bucket steam valve modeling and experimental results at different pressure differences is shown in Fig. 19. The experimental and simulated sound pressure levels show basically the same trend of total frequency. The simulated and experimental sound pressure levels overlap within the range of midfrequency, but the experimental sound pressure level is slightly higher in the high frequency range. The computed sound pressure level is marginally higher in the low frequency band than the observed sound pressure level. Table 4 illustrates that when comparing the numerical simulation findings with the experimental results, the total variation in sound pressure level is less than 3%, while the greatest difference between the simulated and experimental sound pressure levels is less than 6%. Consequently, the multi-frequency band analysis-based numerical simulation approach for inverted bucket steam valve noise presented in this study has a high level of simulation accuracy.

Table 3 ΔP=0.8MPa sound pressure level at each monitoring point

working condition	Sound pressure level in dB(A) at various monitoring points			Total sound pressure level dB(A)
ΔP=0.6MPa	70.32	68.33	62.45	67.03
ΔP=0.8MPa	65.76	67.21	63.55	65.86
ΔP=1.0MPa	60.22	63.56	66.51	62.43

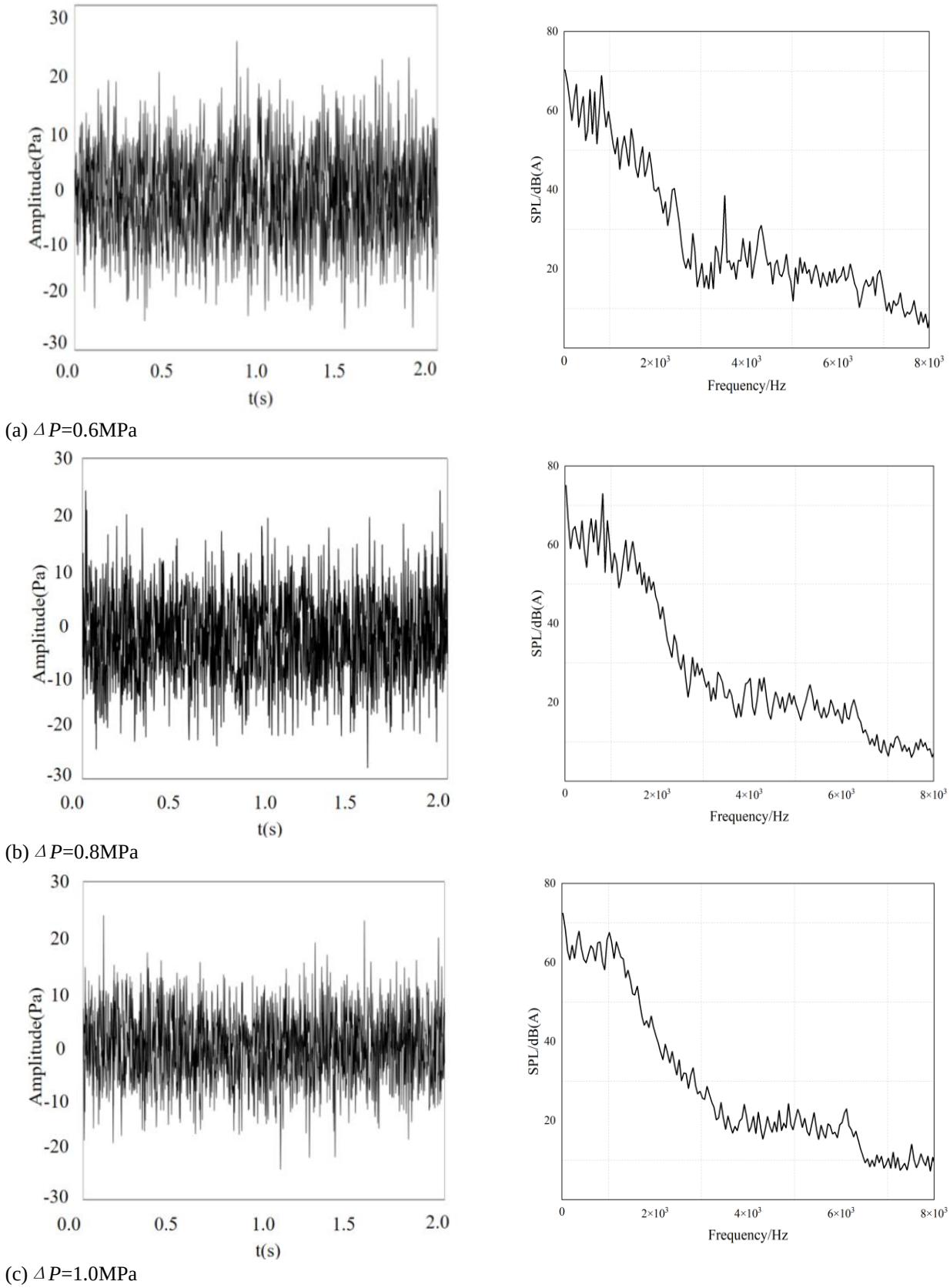

(a) ΔP=0.6MPa

(b) ΔP=0.8MPa

(c) ΔP=1.0MPa

Fig. 18 Time and frequency domain data for the experiment

Table 4 Comparison of experimental and simulated total sound pressure level

Working condition	Δ P=0.6MPa	Δ P=0.8MPa	Δ P=1.0MPa
Simulated total sound pressure level	65.53	64.44	61.21
Experimental total sound pressure level	67.03	65.86	62.43
Error value	2.23%	2.15%	1.95%

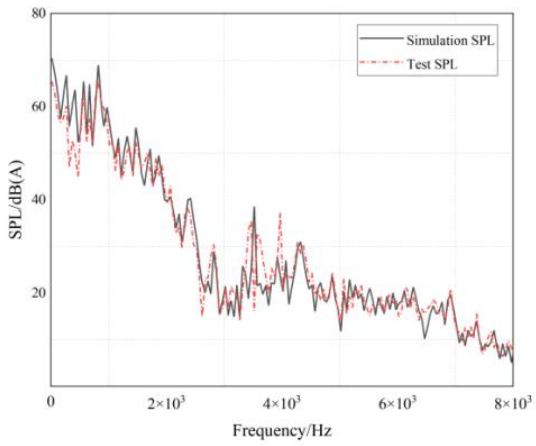

(a) Δ P=0.6MPa

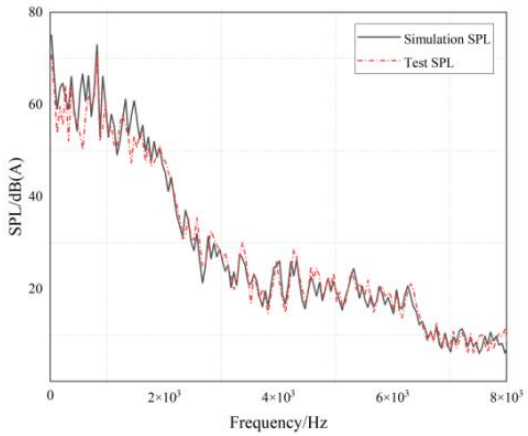

(b) Δ P=0.8MPa

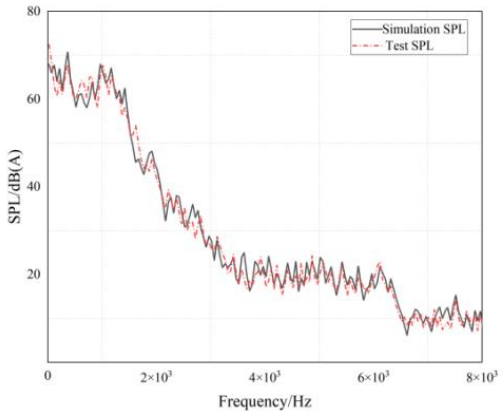

(c) Δ P=1.0MPa

Fig. 19 Comparison of experimental and numerical simulation simulations at different differential pressures

7. CONCLUSIONS

In this paper, focusing on the problem that inverted bucket steam valve noise numerical simulation is difficult to perform and cannot guarantee accuracy, a method based on multifrequency band consideration of inverted bucket steam valve aerodynamic noise numerical simulation is proposed. Aerodynamic noise is simulated for the inverted bucket steam valve at differential pressures of 0.6MPa, 0.8MPa, and 1.0MPa, and the comparison of simulation and experiment data is gathered to confirm the numerical simulation's accuracy. The precision of the numerical simulation is compared with the experimental data in order to verify its correctness. These are the main findings:

(1) The inverted bucket steam valve's internal flow field is examined, and the pressure pulsation that results from simulating the flow field serves as the acoustic stimulation for the numerical simulation of the inverted bucket steam valve's aerodynamic noise. Both the fourth-rated sound source and the even-rated sound source, according to the computation findings, display usual distributions. To demonstrate the numerical simulation method and determine the overall sound pressure level under a pressure difference of 0.8MPa, the working situation with a pressure difference of 0.8MPa. At 0.8MPa, the overall sound pressure level is 64.44dB(A) during numerical simulation.

(2) Through an analysis of the numerical simulation of the aerodynamic noise of the inverted bucket steam valve, it is determined that the noise is primarily caused by the dipole between 2020Hz and 0Hz, and by the combination of the dipole and quadrupole between 2020Hz and 6370Hz. Above 6370Hz, the quadrupole is responsible for the majority of the noise produced by the inverted bucket steam valve.

(3) The method of multifrequency bands was utilized to analyze the numerical simulation results of inverted bucket steam valve aerodynamic noise, and the logarithmic superposition method was employed to derive the numerical simulation results of the total sound pressure level under the three differential pressure conditions. The accuracy of the numerical simulation is demonstrated by the fact that the overall sound pressure level variation between the computational and experimental calculations is less than 3%.

CONFLICT OF INTEREST

The authors have no competing interests and conflicts to disclose.

AUTHOR CONTRIBUTIONS

Man Zhao: Conceptualization, Original draft, Investigation, Software, Formal analysis. **Dan Liu**: Review and editing, Supervision, Project administration. **Jianjun Hou**: Review and editing. **Xuedong Zhang**: Resources. **Shuxun Li**: Review and editing.

REFERENCES

Dai, L., Li, Y., Shang, W., Shi, B., Li, W., & Han, X. (2022). Numerical simulation of aerodynamic noise of small high-speed centrifugal fan. *Noise and Vibration Control*, *42*(03), 49-55. https://doi.org/10.3969/j.issn.1006-1355.2022.03.009

Gao, J., Dong, P., Tan, J., Zhang, L., & Wang, C. (2023). Optimal design of novel honeycomb photocatalytic reactors for numerical analysis of formaldehyde degradation by CFD modeling. *Res Chem Intermed 49*, 1683−1700. https://doi.org/10.1007/s11164-023-04961-4

Guo, H., Wang, Y .S., Zhu, F., Liu, N. N., & Yang, C. (2021). Multi-field coupling prediction for improving aeroacoustic performance of muffler based on LES and FW-H acoustic analogy methods. *International Journal of Aeroacoustics*, *20*(3-4). https://doi.org/10.1177/1475472X211005409

Hou, J., Li, S., Yang, L., Liu, D., & Zhao, Q. (2023). Numerical simulation and reduction of balance valve noise based on considering quadrupole and dipole in different frequency bands. *Applied Acoustics*, *211*. https://doi.org/10.1016/j.apacoust.2023.109504

Huang, X., Zhang, S., Luo, Y., & Zhang, W. (2014). Numercial simulation of a special valve in aerodynamic conveying pipelines. *Advanced Materials Research*, 1070-1072(1070-1072). https://doi.org/10.4028/www.scientific.net/AMR.1070-1072.1963

Li, H., & Guo, H. (2012). Exploration on aerodynamic noise characteristics for control valve of steam turbine. *Applied Mechanics & Materials*, *22*(04), 395-400. https://doi.org/10.4028/www.scientific.net/AMM.224.395

Li, S., Wang, T., Xu, X., Meng, L., & Lou, Y. (2018). Study of vibration characteristics of high-pressure drop sleeve steam valves. *Vibration and Shock*, *37*(04), 147-152. https://doi.org/10.13465/j.cnki.jvs.2018.04.022

Li, S., Xu, D., Li, Q., & Wang, C. (2012). Design and numerical simulation of inverted bucket pilot operated steam valves. *Journal of Irrigation and Drainage Machinery Engineering*, *30*(03), 346-350. https://doi.org/10.3969/j.issn.1674-8530.2012.03.019

Liao, J., Hao, J., Liu, B., Yang, H., & Wang, W. (2022). Aerodynamic noise generation and control mechanism of eccentric rotary valves. *Noise and Vibration Control*, *42*(06). https://doi.org/10.3969/j.issn.1006-1355.2022.06.046

Liu, C., Cao, Y., Ming, P., Sun, W., & Zhang, W. (2018). Numerical prediction of aerodynamic noise in a high-pressure ratio centrifugal compressor. *Journal of Internal Combustion Engine*, *36*(06), 553-560. https://doi.org/10.16236/j.cnki.nrjxb.201806072

Liu, J., Zhang, J., & Zhang, W. (2013). Characterization of aerodynamic noise sources in vacuum tube high-speed trains. *Journal of Vacuum Science and Technology*, *33*(10), 1026-1031. https://doi.org/10.7511/jslx201301016

Mori, M., Masumoto, T., & Ishihara, K. (2014). *Study on modeling of flow induced noise using Lighthill's analogy and boundary element method.* Internoise - international Congress on Noise Control Engineering: Improving the World Through Noise Control. https://acoustics.asn.au/conference_proceedings/INTERNOISE2014/papers/p309.pdf

Mori. M., Masumoto, T., Ishihara, K. (2017). Study on acoustic, vibration and flow induced noise characteristics of T-shaped pipe with a square cross-section. *Applied Acoustics*, *120*, 137-147. http://dx.doi.org/10.1016/j.apacoust.2017.01.022

Qiu, C., Yu, L., Qian, J., & Jin, Z. (2023). Cavitation and noise analysis of sleeve type steam valves under multiple operating conditions. *Journal of Irrigation and Drainage Machinery Engineering*, *41*(03), 281-287. https://doi.org/10.3969 /j.issn.1674 — 8530.21.0071

Shi, H., Zhou, X., Zhou, A., Zhang, B., & Li, S. (2023). Numerical simulation of flow-solid coupling noise in marine three-way control valves. *Applied Acoustics*, http://kns.cnki.net/kcms/detail/11.2121.O4.20230523.1125.002

Si, Q., Sheng, G., Heng, Y., Cui, Q., & Huang, K. (2018). Numerical simulation of flow-induced noise in centrifugal pumps based on Lighthill acoustic analog theory. *Vibration and Shock*, *37*(23), 84-90+97. https://doi.org/10.13465lj. cnki.jvs.2018.23.012

Sim, H. Y., Ramli, R., Saifizul, A., & Soong, M. (2020). Detection and estimation of valve leakage losses in reciprocating compressor using acoustic emission technique. *Measurement*, *152*, 107315. https://doi.org/10.1016/j.measurement.2019.107315

Tan, J., Dong, P., Gao, J., Wang, C., & Zhang, L. (2023). Coupling bionic design and numerical simulation of the wavy leading-edge and seagull airfoil of axial flow blade for air-conditioner. *Journal of Applied Fluid Mechanics*, *16* (7), 1316-1330. https://doi.org/10.47176/jafm.16.07.1634

Tao, H., Lei, W., Cen, K., Bin, S., Rui, S., Hong, L., & Qing, W. (2020). Flow-induced noise analysis for natural gas manifolds using LES and FW-H hybrid method. *Applied Acoustics*, *159*, 107101. https://doi.org/10.1016/j.apacoust.2019.107101

Wang, D., Bai, J., Huang, J., Hua, J., & Dong, J. (2013). Numerical simulation of aerodynamic noise based on turning/scale adaptation model and FW-H acoustic equation. *Journal of Computational Mechanics*, *30*(05), 704-711. https://doi.org/10.7511/jslx201305019

Wang, W., Shi, L., Chai, S., Liu, Y., & Jiang, P. (2007). Calculation and analysis of flow and noise in the main regulating valve of 1000MW supercritical turbine. *Power Engineering*, (03), 401-405. https://doi.org/10.3321/j.issn:1000-6761.2007.03.023

Wu, M., Gao, Y., & Zhang, Y. (2022). Numerical simulation of ball valve leakage flow acoustic field

based on the coupling of SAS and FW-H model. *Ship Science and Technology*, *44*(02), 86-90. https://doi.org/10.3404/j.issn.1672-7649.2022.02.016

Wu, Y., Huang, C., Shen, C., Wang, Z., Liu, J., & Li, S. (2023). Noise characterization of steam engine bypass control valve based on BEM acoustic-fluid-solid coupling. *Chemical Machinery*, *50*(03), 354-360. https://doi.org/10.20031/j.cnki.0254-6094.202303012

Xu, F., & He, E. (2017). Analysis of the mechanism of aerodynamic noise generation and its influencing factors of the valve of aircraft ring control duct. *Journal of Northwestern Polytechnical University*, *35*(04), 608-614. https://doi.org/10.3969/j.issn.1000-2758.2017.04.008

Xu, Z., Wang, D., Wang, Z., Zhang, J., & Chen, H. (2010). Numerical analysis of airflow-induced vibration and noise in main steam isolation valves of nuclear power plants. *Atomic Energy Science and Technology*, *44*(01), 48-53. https://doi.org/CNKI:SUN:YZJS.0.2010-01-010

Yan, B., Jin. H., Huang, C., Shen. H., Hu. Y., & Li, S. (2023). Study on flow excitation resonance of bypass control valve for conventional island steam engine. *Fluid Machinery*, *51*(09). https://doi.org/10.3969/j.issn.1005-0329.2023.09.005

Yuan, Y., Qiu, F., Chen, Y., & Yuan, J. (2017). Experimental study on the noise of steam underwater injection in a closed vessel. *Thermal Power Engineering*, *32*(02), 74-80+138-139. https://doi.org/10.16146/j.cnki.rndlgc. 2017.02.011